JAST, Vol. 5, No. 1, pp 23–33

JAST
Journal of Aerospace Science and Technology

Numerical Simulation of Partial Cavitation over Axisymmetric Bodies: VOF Method vs. Potential Flow Theory

I. Rashidi[1], H. Moin[2], Mohammad P. Fard[3] and Mahmoud P. Fard[4]

A computational study of partial cavitation over axisymmetric bodies is presented using two numerical methods. The first method is based on the VOF technique where transient 2D Navier-Stokes equations are solved along with an equation to track the cavity interface. Next, the steady boundary element method (BEM) based on potential flow theory is presented. The results of the two methods for a disk cavitator are compared with each other and with those of the available experiments and analytical relations. The two methods are then used to predict the partial cavity over an axisymmetric body consisting of a disk cavitator followed by a conical section and ending in a cylindrical shape. The effects of various parameters such as cone length, cone angle, cavitator radius and cylinder diameter are investigated. The results show that as the cone length increases, the cavity region covers a larger portion of the body. Reducing the cone angle increases both the length and diameter of the cavity region. For an axisymmetric body with a larger radius the cavity detachment is more likely to occur.

NOMENCLATURE

English symbols:

$\vec{F}_b$	Body force acting on the fluid per unit volume (N/m^3)
G	Potential function
$\vec{g}$	Gravitational acceleration (m/s^2)
n	Normal vector
P	Pressure (Pa)
q	Volume flow rate (m^3/s)
r	Component of axisymmetric coordinates
S	Mass transfer sink term
s	Arclength along a meridian
t	Time (s)
$\vec{V}$	Velocity vector (m/s)
x	Component of axisymmetric coordinates

Greek symbols:

ϕ	Total velocity potential
φ	Disturbance velocity potential
μ	Viscosity (Kg/m.s)
θ	Poppet angle (degrees)
ρ	Density (Kg/m^3)
σ	Cavitation number

Subscripts:

b	Body
c	Cavity interface
D	Drag force
l	Liquid
v	Vapor
0	detachment point of the cavity

1. *PhD Candidate, Dept. of Mech. Eng., Ferdowsi Univ. of Mashhad, Mashhad, Iran.*
2. *MSc Graduate, Dept. of Mech. Eng., Ferdowsi Univ. of Mashhad, Mashhad, Iran.*
3. *Assistant Professor, Dept. of Mech. Eng., Ferdowsi Univ. of Mashhad, Mashhad, Iran, Email: mp-fard@um.ac.ir.*
4. *Assistant Professor, Dept. of Mech. Eng., Ferdowsi Univ. of Mashhad, Mashhad, Iran.*

∞ Ambient

INTRODUCTION

The cavitation phenomenon is known as liquid vaporization that occurs whenever the liquid pressure falls below its vapor pressure. This phenomenon is categorized with a nondimensional parameter called cavitation number, which is defined as:

$$\sigma = \frac{P_\infty - P_v}{\frac{1}{2}\rho V_\infty^2} \quad (1)$$

where P_v is the vapor pressure, ρ the liquid density, and P_∞, V_∞ are the ambient pressure and inflow velocity, respectively. The cavitation regimes are classified into incipient-, shear-, cloud-, partial- and super-cavitation depending on the cavitation number [1]. The cavitation occurs around axisymmetric bodies at points where the local pressure drops to the environment vapor pressure. Any sudden change in the body shape may cause a pressure rise or fall and, therefore, may be an inception point for cavitation. Although super-cavitation decreases drag forces extensively, when maneuvering of the vehicle is necessary, partial cavitation is more preferable [2]. Also, partial cavities are widely used in ventilated systems [2, 3].

During the last decades, numerous studies have been performed in cavitation using various methods [1]. Cavitation models based on the Navier-Stokes equations emerged in early 1990's. These models are divided into two main categories: interface tracking method and homogeneous equilibrium flow [1, 4]. In interface tracking method, a constant pressure (vapor pressure) is assumed for the cavity region and a wake model is used to predict the shape of the cavity in adaptive grids. In the second category, used in this study, the density field is estimated by various models from which the method based on single-fluid modeling has been shown to be more accurate [1]. In this approach, an advection equation for liquid (or vapor) volume fraction is solved and the density is computed according to the volume fraction of the two phases. This approach has been widely applied to simulate cavitation. The selection of an appropriate mass transfer model and an algorithm for advection equation are the main issues. Yuan *et.al.* [5] suggested a cavitation model based on Rayleigh relation. Singhal *et.al.* [6], Merkle *et.al.* [7] and Kunz *et.al.* [8] have used different mass transfer models based on semi-analytical equations. A well-known method to solve the advection of a free-surface such as a cavity interface is the VOF technique. Frobenius and Schilling [9] as well as Wiesche [10] used this technique to simulate cavitation over hydrofoils and pump impellers. A review of the reported literature reveals that VOF method can accurately capture cavity shape and characteristics. In this study, a modified VOF technique based on Youngs' PLIC algorithm [11] is combined with a mass transfer model of Kunz *et.al.* [8] to simulate cavitation.

A different type of model used by many researchers for studying cavitation is Boundary Element Method (BEM). Early research based on this technique in partial-cavitation flows was performed by Varghese, *et.al.* [2], but they used BEM to solve potential flow for arbitrary bodies after Hess and Smith [12]. Nonlinear BEM method was developed for cavitating flows around hydrofoils by Uhlman [13, 14], and Kinnas and Fine [15, 16]. They distributed sources and normal dipoles along the solid body-cavity interface. The unknown values of these sources and dipoles were determined by imposing the dynamic condition on an assumed cavity boundary. The kinematic boundary condition was then used to update the cavity shape. Beginning in 1994, two numerical hydrodynamics models were developed for axisymmetric supercavitating high-speed bodies: a slender-body theory model (Varghese *et.al.* [17]) and a BEM method (Kirschner *et.al.* [18]; Uhlman *et.al.* [19]). The results of both the slender-body theory and the BEM method have been shown to compare well with other numerical and experimental results. These models can predict the shape and length of cavity, accurately. The BEM method was employed to examine supercavitating flows past disk as well as cone and sigma-shaped cavitators, where good agreements with experimental and analytical results have been reported [20].

In this paper, partial cavitation for water flows over axisymmetric bodies is studied using two general types of models mentioned above. For the VOF method, a modified Young's PLIC algorithm is used to advect the interface between the two phases (cavity). For the BEM method, sources and normal dipoles are distributed along the body-cavity surface. The unknown values of the source and dipole strengths are then obtained using the mixed Fredholm integral equation that results from the application of Green's third identity.

NUMERICAL METHODS

The two methods of VOF and BEM are briefly discussed in this section. The VOF method is based on the solution of the full Navier-Stokes equations along with an equation for the advection of cavity interface. The BEM method, however, is based on the concept of potential flow theory. For the VOF method, the fluid flow is assumed to be Newtonian and laminar. In this study, the main focus is on Supercavitation, where the cavity closes in the liquid. For this phenomenon, turbulence effects are not important. Experimental studies also show that the effects of turbulence are mainly in the cavity closure region and in the shear

flow outside the cavity [1]. Turbulence intensity is increased at the end of the cavity where the reentrant jet is formed; this region, therefore, is turbulent. The flow inside the cavity, however, is laminar. As a result, flow turbulence mainly affects the transient behavior of partial cavitation and the inception of cavitation. In studying the steady behavior of axisymmetric supercavities that closes inside the liquid region rather than on a solid wall, the turbulence is only a second order effect that will not change the numerical solution in general. A manifestation of this point is the good agreement that will be shown later in this paper between the results of the numerical model with those of the experiments.

Volume-of-Fluid Method (VOF)

In this method, the advection of the cavity interface is simulated based on the Volume-of-Fluid (VOF) technique along with a cavitation model for mass transfer between the two phases of liquid and vapor.

VOF Algorithm

The governing equations for the 2D/axisymmetic incompressible fluid flow are:

$$\vec{\nabla}.\vec{V} = 0 \tag{2}$$

$$\frac{\partial \vec{V}}{\partial t} + \vec{\nabla}.\left(\vec{V}\vec{V}\right) = -\frac{1}{\rho}\vec{\nabla}P + \frac{1}{\rho}\vec{\nabla}.\vec{\tau} + \frac{1}{\rho}\vec{F}_b + \vec{g} \tag{3}$$

where $\vec{V}$ is the velocity vector, P indicates the pressure, F_b is body force acting on fluid, $\vec{g}$ is the acceleration due to gravity and τ represents Newtonian viscous stress tensor. In VOF, the phase change boundary is simulated by a scalar field f, whose value is equal to zero in the vapor phase and one in the liquid. When a cell is partially filled with liquid, f has a value between zero and one. The discontinuity in f is propagating through the computational domain according to:

$$\frac{df}{dt} = \frac{\partial f}{\partial t} + \vec{V}.\vec{\nabla}f = S \tag{4}$$

where S is the cavitation mass transfer sink term. This equation with different mass transfer models can be used to simulate many physical phenomena such as cavitation, vaporization, and condensation. The Hirt-Nichols [21] and Youngs-PLIC [11] methods are widely used for the advection of the volume fraction f in Eq. 4. Although the Hirt-Nichols has been used in most cavity simulations, in this study a more accurate method of Youngs is employed. To begin the advection using Eq. 4, an intermediate value of f is introduced as:

$$\tilde{f} = f^n - \delta t\vec{\nabla}.(\vec{V}f^n) \tag{5}$$

and "divergence correction" completes the scheme:

$$f^{n+1} = \tilde{f} + \delta t(\vec{\nabla}.\vec{V})f^n + \delta t(S^n) \tag{6}$$

This scheme initiates the distribution of f for velocity and pressure calculations in each time step. Because a single set of equations is solved for both phases, mixture properties are used as:

$$\rho = f\rho_l + (1-f)\rho_v$$
$$\mu = f\mu_l + (1-f)\mu_v \tag{7}$$

where subscripts l and v denote the liquid and vapor, respectively. Two-step time projection method is employed for the solution of momentum equations. First an intermediate velocity is calculated based on the terms related to advection, viscosity and body forces:

$$\frac{\vec{V}-\vec{V}^n}{\delta t} = -\vec{\nabla}(\vec{V}\vec{V})^n + \frac{1}{\rho^n}\vec{\nabla}.\vec{\tau} + \vec{g}^n + \frac{1}{\rho^n}\vec{F}_b^n \tag{8}$$

Continuum Surface Force (CSF) method [22] is used to treat the surface tension in interfacial cells as a body force. Pressure field is obtained by Poisson equation as:

$$\vec{\nabla}.\left(\frac{1}{\rho}\vec{\nabla}P^{n+1}\right) = \frac{\vec{\nabla}.\vec{V}}{\delta t} \tag{9}$$

Finally, the pressure field is used to compute the new time velocities:

$$\frac{\vec{V}^{n+1}-\vec{V}}{\delta t} = -\frac{1}{\rho}\vec{\nabla}P^{n+1} \tag{10}$$

An Incomplete Cholesky Conjugate Gradient Decomposition (ICCG) solver is employed for solving Eq. 9. Having calculated the new time level pressures, the velocities are updated using Eq. 9.

Figure 1 shows the boundary conditions used in the VOF method. The "in flow" and "out flow" boundary conditions are mathematically written as: $(\vec{\nabla}\vec{V}).\hat{n} = 0$, $(\vec{\nabla}p).\hat{n} = 0$ and $(\vec{\nabla}f).\hat{n} = 0$, whereas "n" refers to the normal vector of the boundary. For the axis of symmetry, no gradient conditions and free-slip boundary conditions are implemented.

Cavitation Model

Several cavitation mass transfer models can be used to replace S in Eq. 4. Among the more recommended

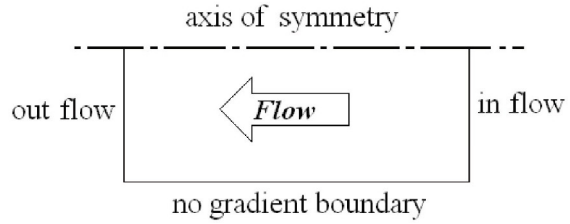

Figure 1. The Boundary conditions used in VOF simulations.

models we have the Rayleigh equation and semi-analytical schemes [1]. Many semi-analytical schemes are based on the modified Rayleigh theory or a mass-momentum interaction model around the cavity interface [23]. In current study, the semi-analytical model of Kunz is used to treat S in Eq. 4:

$$\frac{\partial f}{\partial t}+\vec{V}.\vec{\nabla} f=\frac{C_{dest}\rho_l \min(P_l-P_v,0)f}{(1/2\rho_l V_\infty^2)\rho_v t_\infty}+\frac{C_{prod}(1-f)f^2}{\rho_l t_\infty} \tag{11}$$

where $C_{dest} = 9 \times 10^5$ and $C_{prod} = 3 \times 10^4$ are numerical-experimental weighting coefficients. The flow characteristic time, t_∞, is defined as the ratio of the maximum solid-body diameter to the main flow velocity. The second term in the right hand side of Eq. 11 is for the condensation that occurs near the cavity closure region. This phenomenon causes small vapor structures to detach from the end of the cavity. The Kunz model assumes a moderate rate of constant condensation; therefore, it reconstructs the cavity region more accurately than the other models [1, 23].

Boundary Element Method (BEM)

This section explains the BEM cavitation model based on the potential flow theory.

Mathematical Formulation

The potential flow model presented here is based on Green's third identity formulation [15]. Applying this formulation to the axisymmetric disturbance velocity potential, φ, results in:

$$2\pi\varphi(r,x)=\iint_S \left\{\frac{\partial\varphi}{\partial n}G(x,r;\xi,R) -\varphi(r,x)\frac{\partial G(x,r;\xi,R)}{\partial n}\right\} R\,d\varphi\,ds \tag{12}$$

where n is the normal vector directed outward from the solid-body surface and the cavity interface, s is the arclength along a meridian, and x and r are the components of the axisymmetric coordinate system. $G(x,r;\xi,R)$ is the potential function related to the fluid sources distributed along a ring of radius R located on the axis at $x = \zeta$ (see Figure 1). The potential function is defined as:

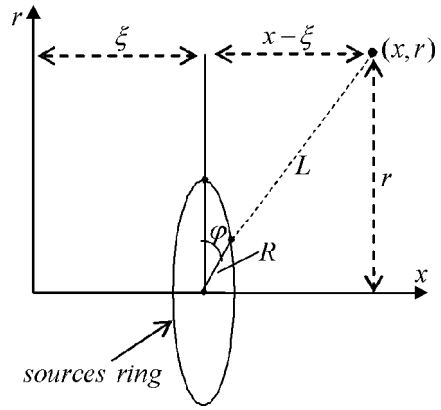

Figure 2. Source ring in a cylindrical coordinate.

$$G(x,r;\xi,R)=\int_{-\pi}^{+\pi}\frac{d\varphi}{\sqrt{(x-\xi)^2+r^2+R^2-2rR\cos(\varphi)}} = RJ_1^0(A,B) \tag{13}$$

where

$$A=r^2+R^2+(x-\xi)^2$$
$$B=2rR \tag{14}$$

and

$$J_1^0(A,B)=\frac{4}{\sqrt{A+B}}K(k)$$
$$K(k)=\int_0^{\frac{\pi}{2}}\frac{d\varphi}{\sqrt{1-k^2\sin^2(\varphi)}}$$
$$k^2=\frac{2B}{A+B} \tag{15}$$

Equation 13 states that the potential flow on any surface can be shown by means of a series of ring-distribution of sources and dipoles. For this purpose, a series of source rings is distributed on the liquid/cavity interface, and a series of dipoles rings on the solid-body/cavity interface (Figure 1). The total and disturbance potentials are related by:

$$\phi = x+\varphi \tag{16}$$

where all quantities are made dimensionless with respect to ρ, U_∞ and d. The boundary conditions are kinematic condition on the solid-body surface. Both the kinematic and dynamic conditions are on the liquid/cavity interface. These conditions are mathematically formulated as:

$$\frac{\partial\phi}{\partial n}=0 \quad \text{on } S_b\cup S_c \tag{17}$$

$$\frac{\partial\phi}{\partial s}=\sqrt{1+\sigma} \quad \text{on } S_c \tag{18}$$

where S_b and S_c are the areas of the solid-body surface and the liquid/cavity interface, respectively. These boundary conditions are equal to:

$$\frac{\partial\varphi}{\partial n}=-x_n \quad \text{on } S_b\cup S_c \tag{19}$$

and

$$\frac{\partial \varphi}{\partial s} = \sqrt{1+\sigma} - x_s \quad \text{on } S_c \tag{20}$$

where n and s are unit vectors normal and tangent to the solid-body/cavity boundary, respectively. The last boundary condition may be integrated to yield:

$$\varphi = \varphi_0 + \sqrt{1+\sigma}\,(s - s_0) - (x - x_0) \quad \text{on } S_c \tag{21}$$

where φ_0, is the potential at the detachment point of the cavity on the solid body.

Governing Integral Equation

Placing the unknowns on the left-hand side and the knowns on the right-hand side, Green's third identity is written as:

$$2\pi\varphi + \iint_{S_b} \varphi \frac{\partial G}{\partial n} dS - \iint_{S_c} \frac{\partial \varphi}{\partial n} G dS = \iint_{S_b} \frac{\partial \varphi}{\partial n} G dS - \iint_{S_c} \varphi \frac{\partial G}{\partial n} dS \tag{22}$$

on the wetted portion of the solid-body/cavity boundary and on the liquid/cavity interface:

$$\iint_{S_b} \varphi \frac{\partial G}{\partial n} dS - \iint_{S_c} \frac{\partial \varphi}{\partial n} G dS = \iint_{S_b} \frac{\partial \varphi}{\partial n} G dS - 2\pi\varphi - \iint_{S_c} \varphi \frac{\partial G}{\partial n} dS \tag{23}$$

Implementing the above boundary conditions, Eq. (22) can be written as:

$$2\pi\varphi + \iint_{S_b} \varphi \frac{\partial G}{\partial n} dS - \iint_{S_c} \frac{\partial \varphi}{\partial n} G dS + \varphi_0 \iint_{S_c} \frac{\partial G}{\partial n} dS + \sqrt{1+\sigma} \left[\iint_{S_c} (s - s_0) \frac{\partial G}{\partial n} dS \right] = -\iint_{S_b} x_n G dS + \iint_{S_c} (x - x_0) \frac{\partial G}{\partial n} dS \tag{24}$$

on the solid body, and Eq. (22) becomes:

$$\iint_{S_b} \varphi \frac{\partial G}{\partial n} dS - \iint_{S_c} \frac{\partial \varphi}{\partial n} G dS + \varphi_0 \left[2\pi + \iint_{S_c} \frac{\partial G}{\partial n} dS \right] + \sqrt{1+\sigma} \left[2\pi (s - s_0) + \iint_{S_c} (s - s_0) \frac{\partial G}{\partial n} dS \right] = -\iint_{S_b} x_n G dS + \left[2\pi (x - x_0) + \iint_{S_c} (x - x_0) \frac{\partial G}{\partial n} dS \right] \tag{25}$$

on the liquid/cavity interface.

In addition to these equations, an auxiliary condition is required for which we impose the condition that the net source strength be equal to the flux through the jet, which may be expressed as:

$$\iint_{S_c} \frac{\partial \varphi}{\partial n} dS = \iint_{S_b} x_n dS \tag{26}$$

RESULTS AND DISCUSSION

The two methods described above were used to investigate various effects associated with an axisymmetric body consisting of a disk cavitator followed by a conical section and ending in a cylindrical shape (Figure 4). The geometry parameters shown in Figure 4 are nondimension-alized based on the cavitator diameter.

To validate the models, the results of the two methods are compared with each other and with those of the available experiments in the literature. Water properties at 25°C are considered in this study.

Model Validation

Although cavitation is a complex two-phase phenomenon, analytical solutions of super-cavitation behind simple obstacles such as a disk or a sphere are available. Reichardt analytical relation [24] for super-cavitation behind axisymmetric cavitator is given by:

$$\frac{l_{cavity,\max}}{d_{cavity,\max}} = \frac{\sigma + 0.008}{\sigma(1.7\sigma + 0.066)} \tag{27}$$

$$\frac{d_{cavity_{\max}}}{D_{cavitator}} = \left[\frac{C_D}{\sigma(1 - 0.132\sigma^{0.5})} \right]^{0.5} \tag{28}$$

where $l_{cavity,max}$ and $d_{cavity,max}$ are the maximum length and diameter of the cavity, respectively, and

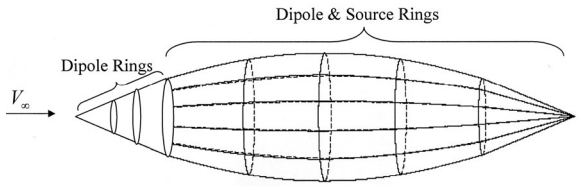

Figure 3. Application of the superposition of the free stream, with distributions of the dipoles and sources rings on the interface of the body/cavity and the liquid/cavity to solve cavitation.

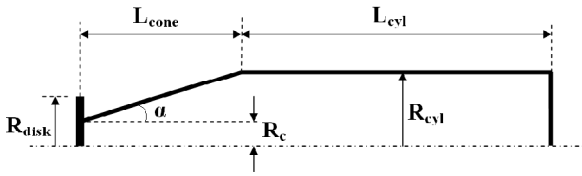

Figure 4. Schematic of the axisymmetric body.

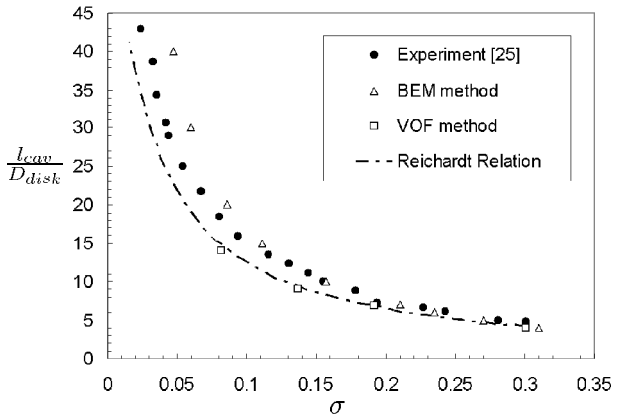

Figure 5. Dimensionless cavity length vs. cavitation number for a disk cavitator.

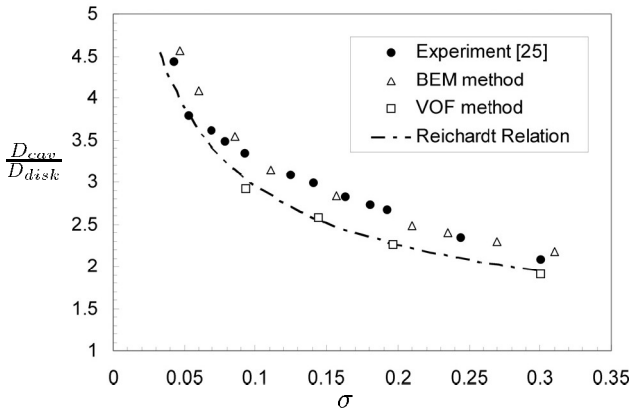

Figure 6. Dimensionless cavity diameter vs. cavitation number for a disk cavitator.

$D_{cavitator}$ represents the maximum diameter of cavitator.

Palset and Schaffer proposed the following analytical equation for the drag coefficient of a disk cavitator for cavitation numbers less than 1.5 [25]:

$$C_D = C_{D_0}(1 + \sigma + 0.028\,\sigma^2) \tag{29}$$

where C_{D_0} is equal to 0.8053.

The cavitation behind a disk cavitator for several cavitation numbers is simulated using both VOF and BEM methods. The results of the two methods are compared with each other and with those of the analytical relations given by Eqs. 27, 28 and 29. Figure 5 compares the results of the two methods with those of the available experiments [1] and Reichardt relation (Eq. 28). As understood from the figure, the results of both models agree well with those of the experiments and the theory for high cavitation numbers ($\sigma > 0.15$). For lower cavitation numbers, while the VOF method predictions are in good agreement with Reichardt relation, the BEM method slightly overpredicts the experimental measurements. The results from different methods and experiments for dimensionless cavity diameter versus cavitation number are shown in Figure 6. The VOF method gives a better prediction compared to that of Reichardt relation (the difference being less than 3.3%). The results of the BEM technique, however, are closer to those of the experiments. The comparison between the two methods, experiments, and Palset-Schaffer equation (Eq. 28) for the drag coefficient is displayed in Figure 7. While the VOF model well predicts the experimental results, the BEM method underpredicts the measurements.

Partial Cavitation over an Axisymmetric Body

In this section, we study the partial cavitation over the axisymmetric body under consideration (Figure 4). The effects of various parameters (cone length, cone angle, and cylinder diameter) on the shape of the cavity for different cavitation numbers are investigated. The results of VOF model for a base case is shown in Figure 8 for a cavitation number of $\sigma = 0.0698$. For this case: R_c=0.25, the cone angle is α=7.407°, and the cylinder radius is R_{cyl}= 0.9. In the VOF method, the full Navier-Stokes equations are solved; therefore, all information regarding the flow is obtained. Figure 8 displays the shape of the cavity along with flow velocity and pressure distributions. The velocity magnitude is seen to be related to the phase of the flow, in the vapor phase the velocity has a smaller magnitude.

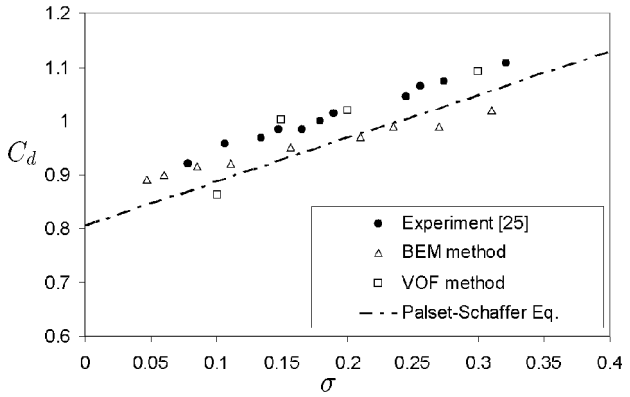

Figure 7. Drag coefficient vs. cavitation number for a disk cavitator.

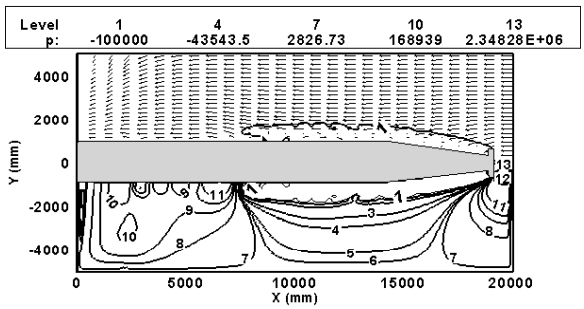

Figure 8. The results of the VOF model for a base case with R_c=0.25 and R_{cyl}= 0.9 for a cavitation number of σ = 0.0698. The image contains cavity shape, velocity and pressure distributions. Pressures shown in this and all the following figures are in Pascal.

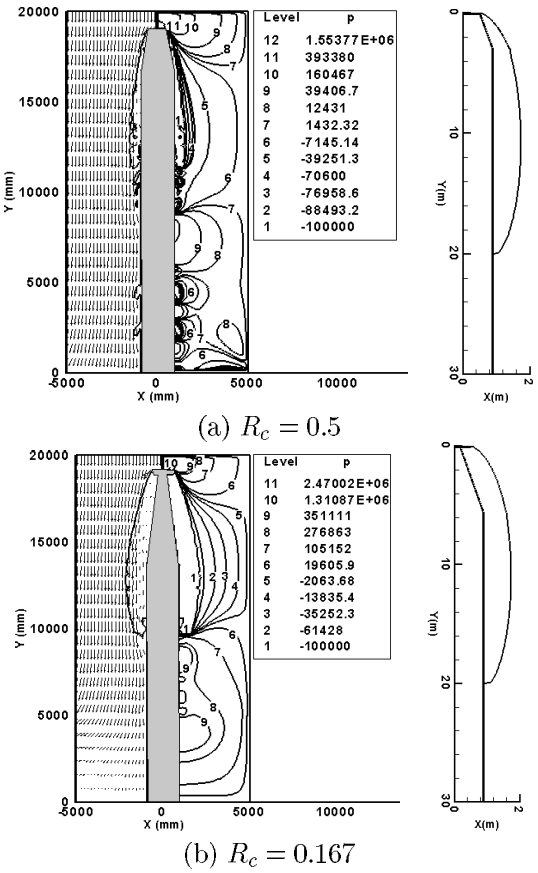

Figure 9. The results of VOF and BEM methods for the effect of cone length (*i.e.* varying R_c at a constant R_{cyl} and cone angle) for a cavitation number of 0.0698.

The reentrant jet at the cavity closure region and the backward flow within the cavity is visible in the figure. The pressure in the vapor phase is seen to be constant and equal to that of the vapor pressure.

To investigate the effects of different geometric parameters, while one parameter is changed from that of the base case, other parameters are held constant. The results for each case are first presented using the VOF method. Then, a quantitative comparison is performed between the two methods of VOF and BEM.

Effect of Cone Length

To study the effect of cone length, the cone angle at α=7.407° and the cylinder diameter at R_{cyl}=0.9 were held constant. Then, by varying R_c (Figure 4), different cone lengths (L_{cone}) were produced. Three different values of R_c were considered for this study. Figure 9 shows the results obtained from the VOF method for two values of R_c equal to 0.167 and 0.5. For the base case shown in Figure 8, R_c was equal to 0.25. A comparison between Figure 8 and the two images of Figure 9 reveals that as the cone length is increased, the cavity region covers a larger space. The case with R_c=0.5 needs extra attention because in this case, the cone length is decreased to the extent that no cavitator exists in front of the body any longer. As seen in Figure 9, the results of both methods indicate that the cavity length does not change significantly when the R_c is changed. The BEM method does not predict the reentrant jet phenomenon; the method needs a more sophisticated model for treating the closure region.

To see the effect of cone length more clearly, the dimensionless cavity length vs. cavitation number for different cone lengths (by varying R_c) are shown in Figure 10, where the results of both the VOF and BEM methods are shown. No experimental or analytical results were available in this case. However, to show the difference between supercavitation behind a disk cavitator (no cylinder) and partial cavitation behind the axisymmetric body under consideration, the results

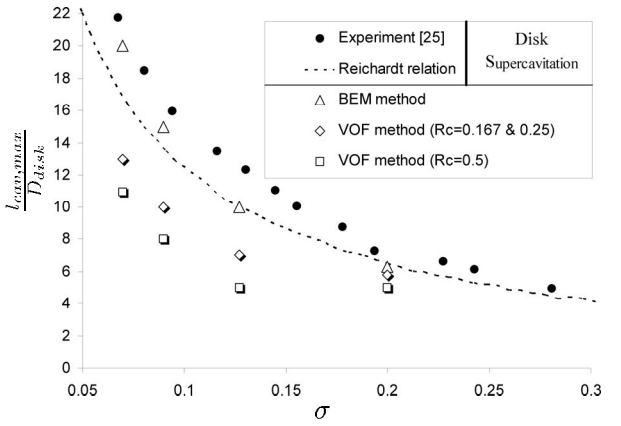

Figure 10. Dimensionless cavity length vs. cavitation number for different cone lengths (by varying R_c). The results are shown using both the VOF and BEM methods. The experimental and analytical results should not be compared with those of the two methods (refer to section of "Effect of Cone Length").

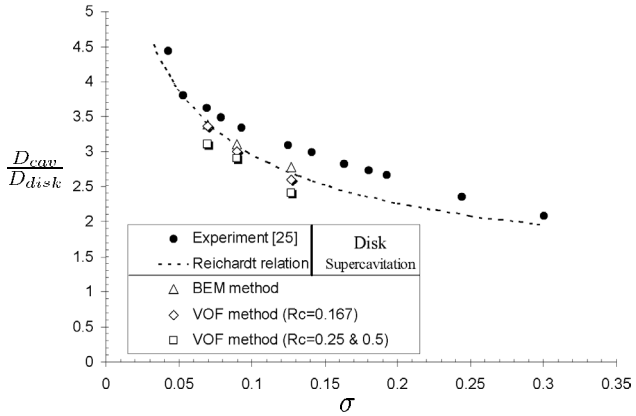

Figure 11. Dimensionless cavity diameter vs. cavitation number for different cone lengths (by varying R_c). The results are shown using both the VOF and BEM methods. The experimental and analytical results should not be compared with those of the two methods (refer to section of "Effect of Cone Length").

of supercavitiaon behind a disk are also displayed in Figure 10. Therefore, the VOF and BEM results in the figure should not be compared with experimental points and the analytical curve shown in the figure. As seen from Figure 10, while in the BEM method, the cone length makes no difference in the cavity length, the VOF method predicts a smaller cavity when the cone length is decreased. As the cavity length is related to the inverse of the cavitation number, when cavitation number increases (*i.e.*, less cavitation) the VOF and BEM results are nearing each other as seen in Figure 10.

Figure 11 shows the dimensionless cavity diameter versus cavitation number for the same geometric variation discussed above (R_c is varying). As observed, the diameter of the partial-cavity predicted by the BEM method does not change with cone length; the results of this method lie in those of the Reichardt relation for supercavitation. The VOF method, however, predicts a smaller value for the cavity diameter compared to that of the BEM. When cavitation number is decreased, the results of the two methods approximate each other.

Effect of Cylinder Radius

The results of the VOF and BEM methods for the shape of the cavity for four different R_{cyls} (nondimensional cylinder radii) are plotted in Figure 12. For the case considered here, the cone angle α was 7.407°, R_c was 0.25 and L_{cyl}+L_{cone} = 40 (see Figure 4). The cylinder radius was R_{cyl}=0.5, 0.7, 0.9, 1.1. As seen from Figure 12, the cylinder radius has no significant effect on cavity length. The cavity diameter, however, is decreased when the cylinder has a larger radius. The cavity detachment from the cylinder is also expected to occur in a cylinder with a smaller radius.

The dimensionless cavitation length vs. cavitation number for two different cylinder radii is plotted in Figure 13. The results of the experiments and theory for supercavitation behind a disk cavitator with radius R_{disk} (*i.e.* with no cone and cylinder body) are also shown. For low cavitation numbers, discrepancies are observed between the results of the two methods (VOF and BEM). The two results, however, agree well when cavitation number increases (σ > 0.2). It can be seen from both methods that when R_{cyl} is decreased, the

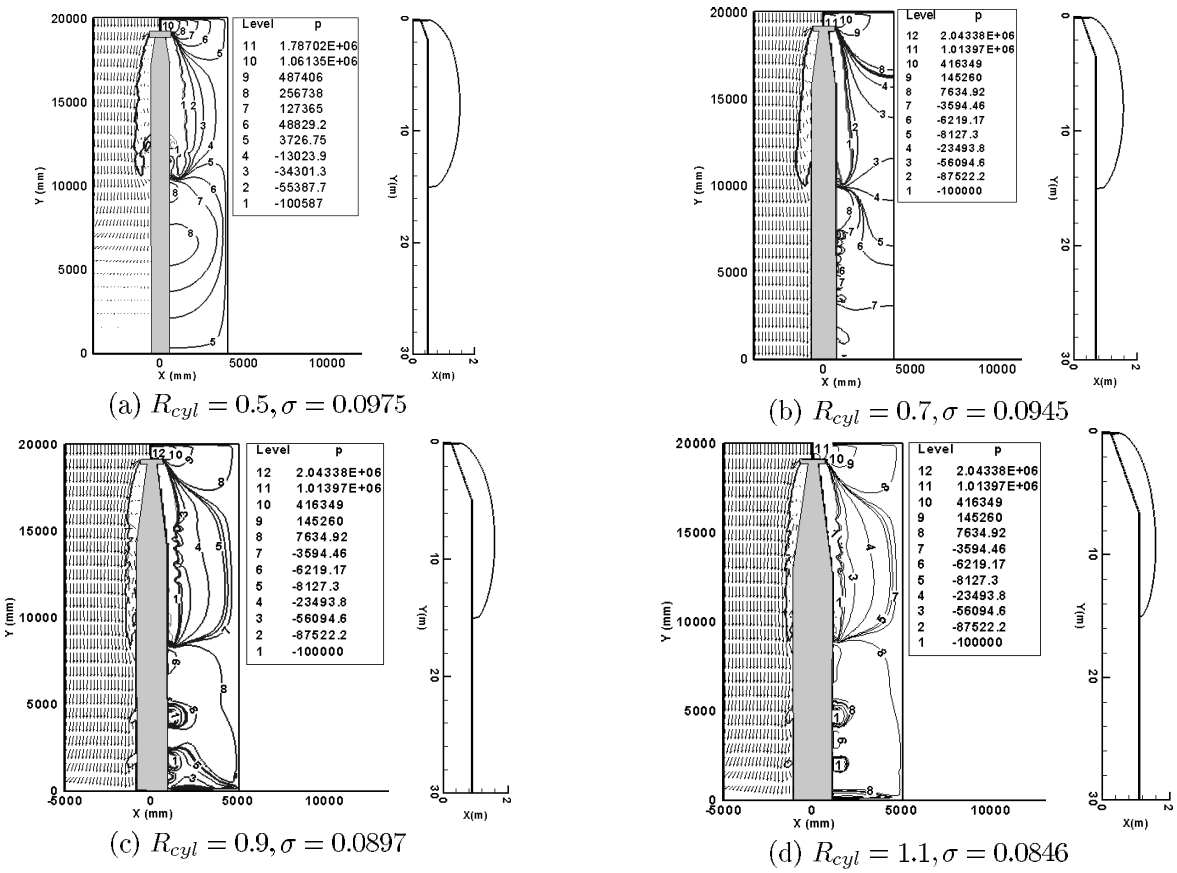

(a) $R_{cyl} = 0.5, \sigma = 0.0975$

(b) $R_{cyl} = 0.7, \sigma = 0.0945$

(c) $R_{cyl} = 0.9, \sigma = 0.0897$

(d) $R_{cyl} = 1.1, \sigma = 0.0846$

Figure 12. The results of the VOF and BEM methods for the effect of cylinder radius (at constant cone angle and R_c) on the characteristics of cavitation for a cavitation number of nearly 0.09.

shape of the cavity approaches that of the supercavity behind a disk cavitator.

The effect of cylinder radius of a constant cone angle on the nondimensional maximum cavity diameter is displayed in Figure 14. While the results of the BEM method follow those of the supercavitation of Reichardt analytical relation, the VOF method predicts a variation of cavity diameter as the cylinder radius is changed. From the results of this method, it appears that the ratio of R_{cyl}/R_{disk} is an important parameter. When R_{cyl} increases, the effect of cavitator diameter on the cavity is reduced.

Effect of Cone Angle

The last effect considered is that of the cone angle for a cylinder with L_{cyl}+L_{cone} = 40 and L_{cone}=5 where R_c was 0.25. Three cone angles of 4^o, 6.3^o, and 10.75^o were considered. Figure 15 displays the results of the VOF and BEM methods for these cases. Reducing the cone angle increases both the length and diameter of the cavity region. It should be mentioned that the reason for the selection of a cavitation number of nearly 0.09 for this figure (and Figure 12) was because in this condition, the effects of geometric parameters and

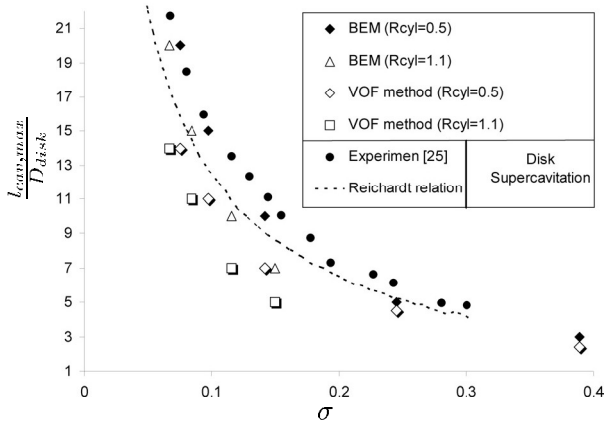

Figure 13. Dimensionless cavitation length vs. cavitation number (R_{cyl}=0.5, 1.1). The experimental and analytical results should not be compared with those of the two methods (refer to section of "Effect of Cone Length").

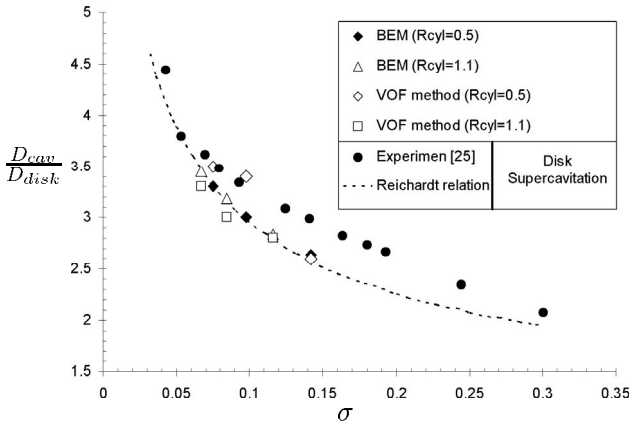

Figure 14. Dimensionless cavitation diameter vs. cavitation number (R_{cyl}=0.5, 1.1). The experimental and analytical results should not be compared with those of the two methods (refer to section of "Effect of Cone Length").

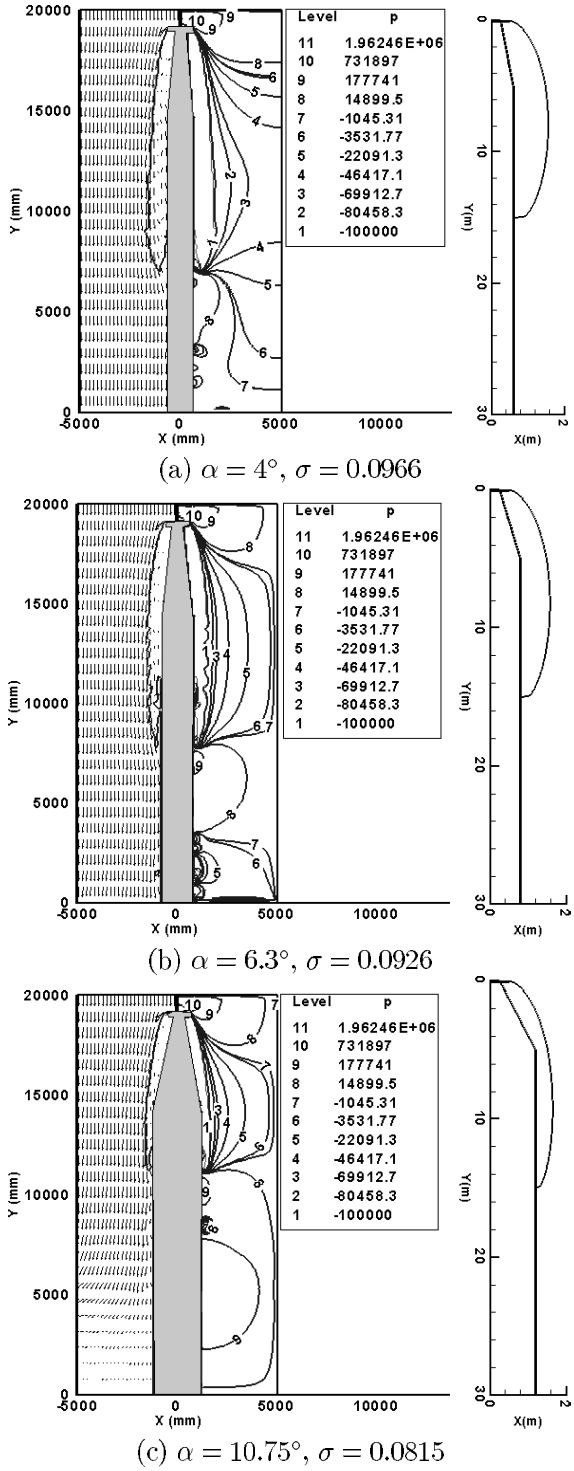

Figure 15. The results of the VOF and BEM methods for the effect of cone angle (at constant R_c) on the characteristics of cavitation for a cavitation number of nearly 0.09.

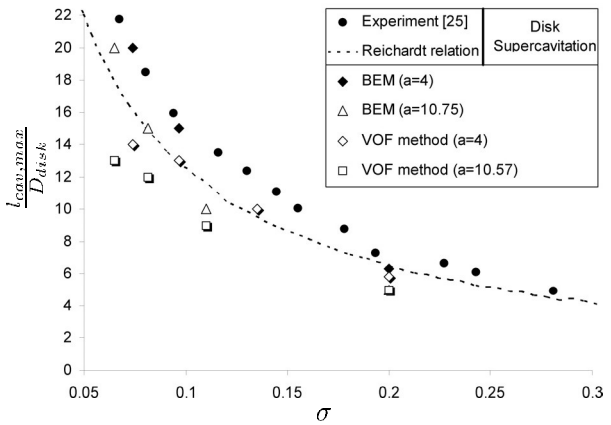

Figure 16. Dimensionless cavitation length vs. cavitation number (α=4°, 6.3°, 10.75° or R_{cyl} = 0.6, 0.8, 1.2); R_c was held constant. The experimental and analytical results should not be compared with those of the two methods (refer to section of "Effect of Cone Length").

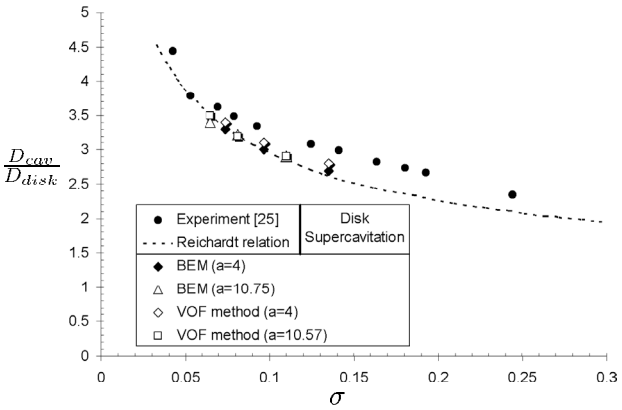

Figure 17. Dimensionless cavitation diameter vs. cavitation number (α=4°, 6.3°, 10.75° or R_{cyl} = 0.6, 0.8, 1.2); R_c was held constant. The experimental and analytical results should not be compared with those of the two methods (refer to section of "Effect of Cone Length").

the comparison between the two methods of VOF and BEM are more clearly visible.

Figure 16 shows the dimensionless cavity length vs. cavitation number for two different cone angles. Similar to the previous figures, the experimental and theoretical results for supercavitation behind a disk cavitator are also plotted in the figure. As observed, the cavity length decreased when the cone angle increased for the same cavitation number. Differences between the two methods of VOF and BEM are seen at low cavitation numbers. However, when σ is greater than 0.2, the results get closer to each other.

The effect of cone angle (at constant R_c) on the cavity diameter is observed in Figure 17. The predictions from both methods are close to each other and to those of the Reichardt analytical relation for the supercavity condition. Therefore, it can be stated that the cone angle has no significant effect on the maximum cavity diameter.

CONCLUSION

In this paper, the partial cavitation over axisymmetric bodies is studied using two numerical methods: the VOF technique based on the solution of the Navier-Stokes equations along with an equation for liquid volume fraction, and boundary element method (BEM) based on the potential flow theory. The following summarizes the main achievements of this study:

1. The results of the two methods agree well with each other and with those of the experiments and theory for a disk cavitator.
2. For an axisymmetric body with a front cavitator, while the two results are in good agreement for large cavitation numbers, discrepancies are seen for a cavitation number less than 0.2.
3. The effects of various parameters such as cone length, cone angle, and cylinder diameter on the shape of the cavity are investigated.
4. The effect of cone length is studied for a partial cavity over an axisymmetric body consisting of a disk cavitator followed by a conical section and ending in a cylindrical shape. Three different values of R_c (Figure 4) were considered for this study. The results reveal that as the cone length increases, the cavity region covers a larger space.
5. Moreover, the shape of partial cavitation for four different values of R_{cyl} is simulated in this paper. As seen, the cylinder radius has no significant effect on cavity length. The cavity diameter, however, is decreased when the cylinder has a larger radius. The cavity detachment from the cylinder is also expected to occur in a cylinder with a smaller radius.
6. The last effect considered is that of the cone angle. Reducing the cone angle increases both the length and diameter of the cavity region.

REFERENCES

1. Passandideh-Fard M. and Roohi E., "Transient Simulations of Cavitating Flows using a Modified Volume-of-Fluid (VOF) Technique", *Int. J. of Comput. Fluid Dynamics*, (2008).
2. Abraham N. Varghese, James S. Ohlman and Ivan N. Kirschner, "High-speed Bodies in Partially Cavitating Axisymmetric Flow", *In proceedings of Fifth International Symposium on Cavitation (CAV2003)*, Osaka, Japan, (2003).
3. Xiaoxing P., Zhi W., Sensen P. and Kai Y., "Generation Mechanism of Ventilated Supercavitation in

an Axisymmetric Body with Cavitator", *In proceedings of Sixth International Symposium on Cavitation, CAV2006*, Wageningen, The Netherlands, (2006).

4. Wang G., Senocak I., Shyy W., Ikohagi T., and Cao S., "Dynamics of Attached Turbulent Cavitating Flows", *Progress in Aerospace Sciences*, **37**, PP 551-581(2001).
5. Yuan W., Sauer J. and Schnerr G.H., "Modeling and Computation of Unsteady Cavitation Flows in Injection Nozzles", *J. of Mechanical Ind.*, **2**, PP 383-394(2001).
6. Singhal N.H., Athavale A.K., Li M., and Jiang Y., "Mathematical Basis and Validation of the Full Cavitation Model", *J. of Fluids Engineering*, **124**, PP 1-8(2002).
7. Merkle C.L., Feng J., and Buelow P.E.O., "Computational Modeling of the Dynamics of Sheet Cavitation", *in Proceedings of the 3rd International Symposium on Cavitation, (CAV1998)*, Grenoble, France, (1998).
8. Kunz R.F., Boger D.A., Stinebring D.R., Chyczewski T.S., Lindau J.W., and Gibeling H.J., "A Preconditioned Navier-Stokes Method for Two-Phase Flows with Application to Cavitation", *Computers & Fluids*, **29**, PP 849-875(2000).
9. Frobenius M. and Schilling R., "Three-Dimensional Unsteady Cavitating Effects on a Single Hydrofoil and in a Radial Pump- Measurement and Numerical Simulation", *in Proceedings of the 5th International Symposium on Cavitation*, Osaka, (2003).
10. Wiesche S., "Numerical Simulation of Cavitation Effects Behind Obstacles and in an Automotive Fuel Jet Pump", *Heat Mass Transfer*, **41**, PP 615-624(2005).
11. Youngs D.L., "Time Dependent Multi Material Flow with Large Fluid Distortion", *Num. Methods for Fluid Dynamics*, PP 273-285.
12. Hess J.L., Smith A.M.O., "Calculation of Potential Flow about Arbitrary Three-Dimensional Bodies", *Progress in Aeronautical Science*, New York, **8**, PP 1-138(1966).
13. Uhlman J.S., "The Surface Singularity Method Applied to Partially Cavitating Hydrofoils", *J Ship Research*, **31(2)**, (1987).
14. Uhlman J.S., "The Surface Singularity or Boundary Integral Method Applied to Supercavitating Hydrofoils", *J Ship Research*, **33(1)**, (1989).
15. Kinnas S.A., and Fine N.E., "Nonlinear Analysis of the Flow Around Partially and Super-Cavitating Hydrofoils by a Potential Based Panel Method", *Proceedings of the IABEM-90 Symposium, International Association for Boundary Element Methods*, Rome, Italy, (1990).
16. Kinnas S.A., and Fine N.E., "A Numerical Nonlinear Analysis of the Flow Around Two- and Three-Dimensional Partially Cavitating Hydrofoils", *J Fluid Mech*, (1993).
17. Varghese A.N., Uhlman J.S., and Kirschner I.N., "Axisymmetric Slender-Body Analysis of Supercavitating High-Speed Bodies in Subsonic Flow", *Proceedings of the Third International Symposium on Performance Enhancement for Marine Applications*, (1997).
18. Kirschner I.N., Uhlman J.S., Varghese A.N., and Kuria I.M., "Supercavitating Projectiles in Axisymmetric Subsonic Liquid Flows", *Proceedings of the ASME & JSME Fluids Engineering Annual Conference & Exhibition, Cavitation and Cavitation and Multiphase Flow Forum*, (1995).
19. Uhlman J.S., Varghese A.N., and Kirschner I.N., "Boundary Element Modeling of Axisymmetric Supercavitating Bodies", *Proceedings of the 1st Symposium on Marine Applications of Computational Fluid Dynamics*, Hydrodynamic/Hydroacoustic Technology Center, McLean, VA, (1998).
20. Savchenko Y.N., Semenenko V.N., Naumova Y.I., Varghese A.N., Uhlman J.S., and Kirschner I.N., "Hydrodynamic Characteristics of Polygonal Contours in Supercavitating Flow", *Proceedings of the Third International Symposium on Performance Enhancement for Marine Applications*, (1997).
21. Katz J. and Matsumoto Y., *Multiphase Flow Forum*, Hilton Head Island, (1994).
22. Hirt F.H. and Nichols B.D., "A Computational Method for Free Surface Hydrodynamics", *J. Comput. Phys.*, **39**, PP 201(1981).
23. Brackbill J.U., Kothe D.B. and Zamach C., "A Continuum Method for Modeling Surface Tension, Comp. Physics", *J. Comput. Phys.*, **100**, PP 335-354(1992).
24. Senocak I. and Shyy W., "Evaluation of Cavitation Models for Navier-Stokes Computations", *Proceeding of FEDSM 02, ASME Fluid Engineering Division Summer Meeting*, Montreal, Canada, (2002).
25. Franc J.P. and Michel J.M., *Fundamentals of Cavitation, Section: 6*, Kluwer Academic Publisher, (2004).